Improved Active Disturbance Rejection Control based on PSO for a Precise Rotating Servo System

Zhenxin He, Jie Wang *, Xiangyang Li, Zhili Zhang, Liang Li

Xi'an Research Institute of High Technology, Department of Precision Instrument, Baqiao District, Tongxin Road, Xi'an City, Shaan Xi Province,710025, China.

* jack_wangjie@163.com

Abstract. The precise rotating servo system is a nonlinear system and demands on high tracking precision and stabilization, so it is difficult to achieve an ideal control result using PID control strategy. An active disturbance rejection control (ADRC) strategy is presented to guarantee the state variables of the closed loop system to converge to the reference input. After arranging the transient dynamics of the desired attitude, we design an extended state observer (ESO) to estimate the impact from parametric uncertainties and disturbances, and the corresponding compensations can be performed online. Then a nonlinear state error feedback law (NLSEF) is designed to reject the tracking error and nonsingular terminal sliding mode control (NTSM) is an effective error combination form to restrain the chattering effectively and keep the system within finite time. To simply the parameters tuning process of ADRC, particle swarm optimization (PSO) is introduced to optimize the parameters of the controller. Simulation results show that the improved ADRC controller has the advantages of high precision and high disturbance rejection ability, which can meet the requirements of measurement precision and stability of the theodolite.

Keywords: ADRC; ESO; NLSEF; NTSM; PSO.

1. Introduction

Electronic theodolite is widely used in the fields of geodetic surveying, weapon system, and engineering surveying. [1] It has been observed that, in the theodolite surveying systems, full automation has been a predominantly attempted domain due to its explicitly military implication and engineering background. [2,3] Theodolite precision rotating servo control is put forward taking shaft motor drive as the core to improve theodolite measure precision and automation degree by combining theodolite with servo drive technology, which is like other automatic orientation measurement system or automatic target acquisition system. [4,5] So, the rotation controller is a very important part of automatic theodolite which has an important effect on its tactical and technical performance. However, the control of a precise rotating servo system is a formidable problem, because accuracy, stability and speed of response are essential to mission accomplishment. Furthermore, the rotating control system should not only have high tracking precision and good dynamic quality, but also have strong robustness to overcome the parameters perturbation and outside disturbance. It is easy to describe the basic principle of theodolite rotating stability, but it is very difficult to realize as there are parameters perturbation, outside disturbance and many nonlinear factors in the regulator system. In order to overcome these problems, a valid control strategy must be established to guarantee the rotating precision and system stability.

The majority of control systems are operated by PID controllers, well before classical and modern control theory were born. At present, PID controller and its improved forms are used to drive the shaft of electronic theodolite. Combining the advantages of traditional PID control with that of fuzzy control, the rotating controller of north seeker theodolite based on adaptive Fuzzy-PID is designed shown in Ref. [6]. Kunming Wang, et al proposed PIDNN control for theodolite rotating servo system. [7] With the neural network (NN) strong approximation, the adverse control effect of model parameters perturbation is effectively compensated. Meanwhile, many kinds of modern control theories, to a great extent, are not realistic as they demand an accurate mathematical model which is not possible to be obtained in some specific conditions. [8]

The application of ADRC and its actual implementation to electronic theodolite rotating control is, we believe, novel. ADRC is a new nonlinear algorithm used in servo system in recent years. It

maintains the advantages of PID, and is introduced into the motion control system by Ref. [17]. There are four fundamental technical limitations in the existing PID framework, and ADRC is very good to deal with these problems, including the following: (1) a simple differential equation to be used as a transient profile generator; (2) a noise-tolerant tracking differentiator; (3) the power of nonlinear control feedback; and (4) the total disturbance estimation and rejection. [18] The purpose of this paper is to show ADRC control has advantages of high precision and high disturbance rejection ability for rotating system by a reasonable mathematical model and some simulation results.

Based on the parameters tuning analysis of ADRC, we know many parameters are needed to be tuned for ADRC, so the parameters influence mutually and the parameters tuning is relatively difficult. In this paper, PSO algorithm is introduced to optimize the parameters of the controller. Meanwhile, NLSEF law adopts NTSM control method with the reaching law to improve the control performance of system. [19]

All manuscripts must be in English, also the table and figure texts, otherwise we cannot publish your paper. Please keep a second copy of your manuscript in your office. When receiving the paper, we assume that the corresponding authors grant us the copyright to use the paper for the book or journal in question. Should authors use tables or figures from other Publications, they must ask the corresponding publishers to grant them the right to publish this material in their paper.

2. Problem Statement

A rotating servo system for automatic electronic theodolite has been designed and built, which can achieve automatic searching and collimation of surveying object, and accomplish automatic measuring with direct and inverted position of telescope, as shown in Figure 1. It consists of the telescope and sighting, the horizontal shaft and vertical shaft, DC motor and transmission device.

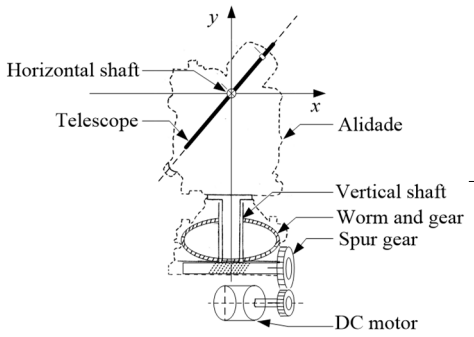

Fig.1. The rotating system of electronic theodolite.

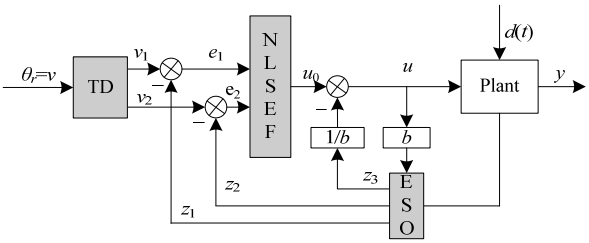

Fig.2. The configuration of the ADRC for theodolite rotating servo system

A DC torque motor is used for the vertical shaft driving device of theodolite rotating servo system. Considering the disturbances, the motor model can be composed by mechanical equation and electrical equation as follows,

$$J\ddot{\theta} = T_e - k_v\omega_s - T_l \tag{1}$$

$$u = r_a i + L_a \frac{di}{dt} + k_e\omega_s \tag{2}$$

$$T_e = k_T i \tag{3}$$

where ra, La, i represent the armature resistance, inductance and current respectively; kT is the motor torque coefficient, kv is the viscous friction coefficient, and ke is the counter voltage factor; J denotes the total moment of inertia of motor Jm and load Jl; Tl is the comprehensive disturbance

including motor friction torque, motor torque fluctuation, system parameter uncertainty and other disturbance; Te is the motor output torque; u is the controller output, which is also regarded as the input control voltage of motor; θ is the actual angular position of motor; ωs is the actual angular velocity of motor.

With the small La, the theodolite rotating servo system can be simplified and expressed in the state space form based on the transfer function, as follows,

$$\begin{cases} \dot{\theta} = \omega_s \\ \dot{\omega}_s = a\omega_s + bu(t) - T_f(t)/J - T_w(t)/J + d(t) \end{cases} \tag{4}$$

where a=-($k_e k_T/(r_a J)$+ k_v/J), b=$k_T/(r_a J)$. $d(t)$ denotes the external kinematic disturbance; $T_f(t)$ denotes the friction torque and $T_w(t)$ is the motor torque fluctuation, which can be described as follows,

$$T_f = [f_c + (f_s - f_c)\exp(-\left|\frac{\omega_s}{\omega_0}\right|^2)]\mathrm{sgn}(\omega_s) \tag{5}$$

where ω_0 is the Stribeck velocity; f_c and f_s represent the levels of Coulomb friction and stiction, respectively.

$$T_w = A_{ripple}\sin(2\pi ft + \varphi), \tag{6}$$

where f=$N\omega_s/360$, A_{ripple} is the amplitude value of torque fluctuation. N is the tooth-slot number, and φ is the phase angle which is relative with initial position of motor.

The angular position and angular velocity are two important variables of the system. Defining the angular position and angular velocity as the system state variables, i.e., $[x_1,x_2]^T$ =$[\theta, \omega_s]^T$, so the mathematic model of theodolite rotating control system can be expressed as the following second-order system,

$$\begin{cases} \dot{x}_1 = x_2 \\ \dot{x}_2 = f(x_1, x_2, d(t), t) + bu(t) \\ y = x_1 \end{cases} \tag{7}$$

where x1=y=θ is the output variable, x2 is magnification factor and d(t) is the external disturbance. f(x1,x2,d(t),t) is the total external and internal disturbances function. Define the error er=yr-y, where yr is reference angular position input.

3. Active Disturbance Rejection Control

Theodolite rotating controller can be designed by classical control theory, such as PID, so the controller design depends heavily on the models. As the plant's parameters vary largely, it is difficult to keep the original good dynamic and static performances.

In this paper, ADRC is employed to control the precise rotating servo system by dealing with modeling errors and structural uncertainties. The structure of control system based on ADRC with *2*th order is shown in Fig. 2, in which three components: (1) Tracking Differentiator (TD), (2) Extended State Observer (ESO), and (3) Nonlinear State Error Feedback (NLSEF) are included. A transitional process and differential signal can be obtained with TD; estimations of the states of plant and disturbances from inside and outside can be obtained with ESO; state errors are combined in non-linear form with NLSEF.

3.1 TD

In the transition design, both the transition signal v_1 and its derivative v_2 are simultaneously presented. The differential signal is usually obtained by the backward difference of the given signal, but it will get unstable and inaccurate results in the presence of noise. However, TD has the ability to

resolve the problem of differential signal extraction via integration to avoid unnecessary noise and make the system performance more effective and robust in some situations. [20] One feasible second-order TD can be designed as follows,

$$\begin{cases} \dot{v}_1 = v_2 \\ \dot{v}_2 = fhan(v_1 - v(t), v_2, r, h_0) \end{cases} \tag{8}$$

where $v(t)$ denotes the control objective. v_1 is the desired trajectory and v_2 is its derivative. r and h_0 are the controller's parameters. r is the speed factor and it will decide tracking speed. h_0 is the filtering factor, which makes an effort of filter. These parameters can be adjusted individually according to the desired speed and smoothness. $fhan(v_1\text{-}v(t),v_2,r,h_0)$ is defined as follows(9).

TD with nonlinear feedback combination can provides transition process for expected input v, that is, v_1 and its differential v_2. Meanwhile, TD has the ability to track the given input reference signal with quick response and no overshoot.

$$\begin{cases} d = rh_0^2, \quad a_0 = h_0 v_2, \quad y = (v_1 - v(t)) + a_0 \\ a_1 = \sqrt{d(d + 8|y|)} \\ a_2 = a_0 + \mathrm{sign}(y)(a_1 - d)/2 \\ s_y = (sign(y + d) - sign(y - d))/2 \\ a = (a_0 + y - a_2)s_y + a_2 \\ s_a = (sign(a + d) - sign(a - d))/2 \\ fhan = -r(\dfrac{a}{d} - sign(a))s_a - rsign(a) \end{cases} \tag{9}$$

3.2 ESO

For the nonlinear system

$$\begin{cases} \dot{x}_1 = x_2 \\ \dot{x}_2 = f(x_1, x_2, t) + bu(t) \\ y = x_1 \end{cases} \tag{10}$$

in order to track the system states x1(t), x2(t) well, the following nonlinear states observer can be designed, [21]

$$\begin{cases} e_0 = z_{01} - y \\ \dot{z}_{01} = z_{02} - \beta_{01} e_0 \\ \dot{z}_{02} = -\beta_{02} fal(e_0, \alpha_1, \delta) + b_0 u \end{cases} \tag{11}$$

where z_{01}, z_{02} are the states observer outputs and β_{01}, β_{02} are the observer gains. $fal(x,\alpha,\delta)$ is a nonlinear function described by

$$fal(x, \alpha, \delta) = \begin{cases} \dfrac{x}{\delta^{1-\alpha}}, & |x| \le \delta \\ sign(x)|x|^{\alpha}, & |x| > \delta \end{cases} \tag{12}$$

The acceleration $f(x_1(t), x_2(t))$ is extended to the new variable x_3, named,

$$x_3(t) = f(x_1(t), x_2(t)) \tag{13}$$

Furthermore, we define $\dot{x}_3(t) = a(t)$. The new extended system from the system (10) can be now rewritten as follows,

$$\begin{cases} \dot{x}_1 = x_2 \\ \dot{x}_2 = x_3 + bu \\ \dot{x}_3 = a(t) \\ x_1 = y \end{cases} \tag{14}$$

Now, for the above extended system, we construct a state observer in the form as follows,

$$\begin{cases} e = z_1 - y \\ \dot{z}_1 = z_2 - \beta_1 e \\ \dot{z}_2 = z_3 - \beta_2 fal(e, \alpha_1, \delta) + b_0 u \\ \dot{z}_3 = -\beta_3 fal(e, \alpha_2, \delta) \end{cases} \tag{15}$$

where z_1, z_2, and z_3 are the observer outputs and β_1, β_2, β_3 are the observer gains. By selecting rationally β_1, β_2, and β_3, which is a particular problem, this system can estimate the states variables x_1 and x_2 of the system (10) and the real-time action of the extended state $x_3(t)=f(x_1(t),x_2(t))$, that is, z_1 is used to estimate x_1, z_2 is used to estimate x_2, and z_3 is the extended state variable to estimate the nonlinear part $f(x_1(t),x_2(t))$.

$$x_3(t) = f(x_1(t), x_2(t), t, d(t)) \tag{16}$$

If the function $f(x_1,x_2)$ include the time variable t and the unbeknown disturbance $d(t)$, similarly, supposing that, the observer can also obtain the estimates $z_1(t)$, $z_2(t)$ of the system state variables $x_1(t)$, $x_2(t)$, and the estimate z_3 of the extended state variable $a(t)=f(x_1(t),x_2(t),d(t),t)$. The state observer of the extended system (15) is called the extended state observer (ESO), and the variable $x_3(t)$ is called the extended state.

The structure diagram of ESO is given in Fig. 3,

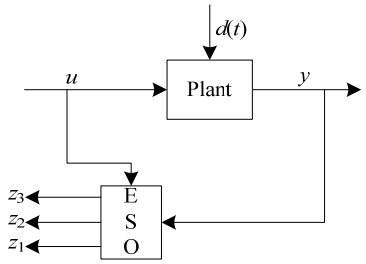

Fig. 3. The structure diagram of ESO.

3.3 Nonlinear Feedback Combination

Based on the system state errors from ESO and TD, feedback control law u can be gotten. A nonlinear combination of error signal and its differential can be constructed as follows,

$$u_0 = k_p fal(e_1, \alpha_1, \delta) + k_d fal(e_2, \alpha_2, \delta) \tag{17}$$

where k_p and k_d are two coefficients of u_0, respectively. $e_1=x_1-z_1$, and $e_2=x_2-z_2$.

Generally, the nonlinear coefficient α_1 and α_2 are selected as $0<\alpha_1<1<\alpha_2$.

At last, the control law can be represented as follows,

$$u = u_0 - \frac{z_3}{b_0} \tag{18}$$

where b_0 is the control compensation coefficient, it requires $b_0<b$, but the different value is small.

4. Simulation Analysis

Aimed at the theodolite rotating system (7), in this section some simulation researches are accomplished to illustrate the feasibility and effectiveness of ADRC and to find some rules of ADRC. The values of the system main parameters are listed in Tab. 1.

Tab. 1 Main parameters of theodolite rotating system

System Parameters		
Rated motor voltage /V	U_0	9
Motor armature resistance /Ω	r_a	2.76
Motor torque coefficient /Nm/A	k_T	1.2
Viscous friction coefficient	k_v	0.2
Counter voltage factor	k_e	0.7
System moment of inertia /Kgm^2	J	0.2
Coulomb friction/Nm	f_c	2.0
Coulomb stiction/Nm	f_s	2.6
Stribeck velocity	ω_0	0.06
Number of pole pairs	P	4
Motor EMF coefficient /V/(rad/s)	k_e	0.7
Torque fluctuation amplitude/Nm	A_{ripple}	0.154
Tooth-slot number	N	79
Phase angle /º	φ	0
Sampling time/sec	T	0.001
ADRC Parameters		
Nonlinear coefficient of *fal*	α_1	0.75
Nonlinear coefficient of *fal*	α_2	1.25
Control compensation coefficient	b_0	1.7
Linear area of *fal*	δ	0.2

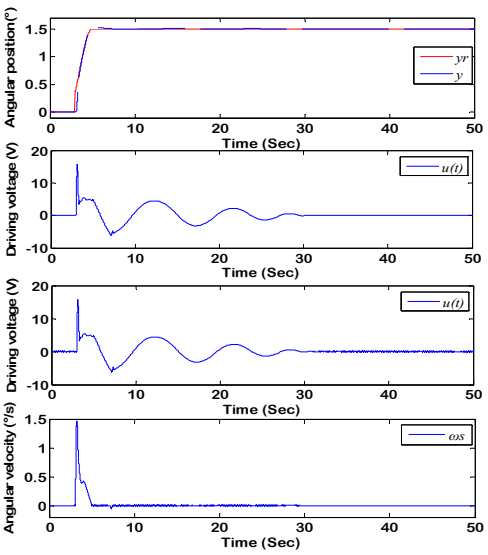

(a) ω_0=5

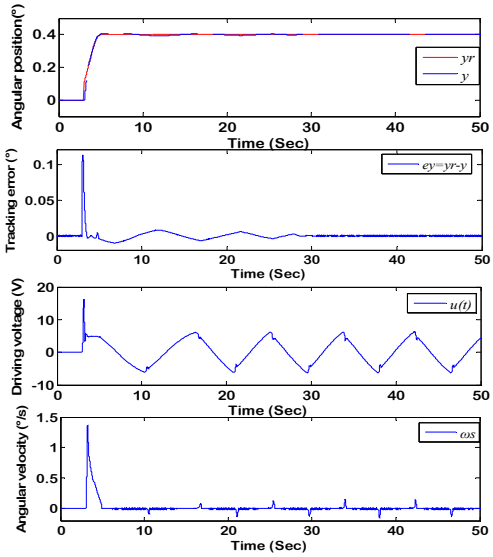

(b) ω_0=10

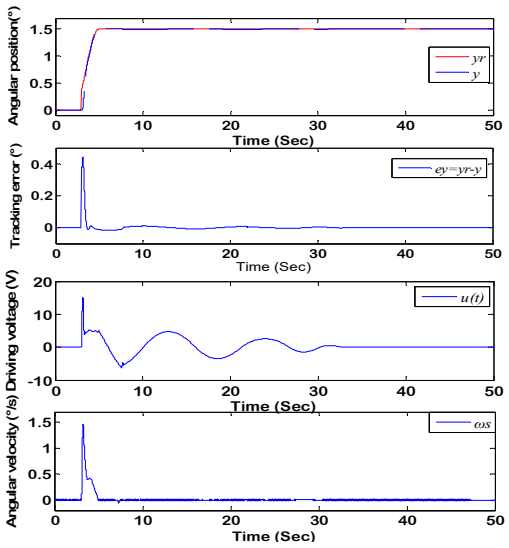

(c) ω_0=20

Fig. 4. The system responses of theodolite angular position tracking with different ω_0.

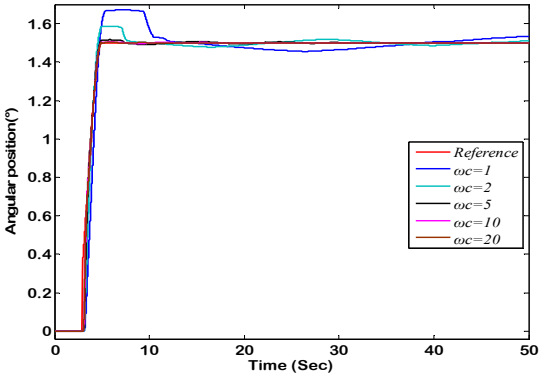

(a) Angular position.

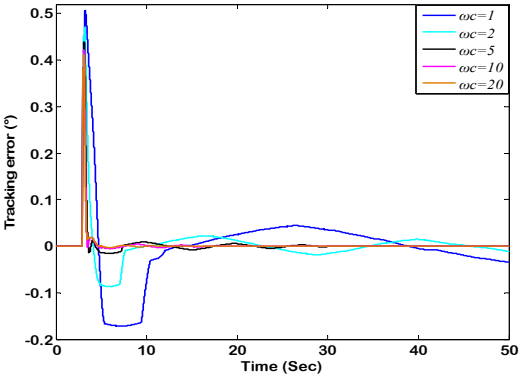

(b) Angular position tracking error.

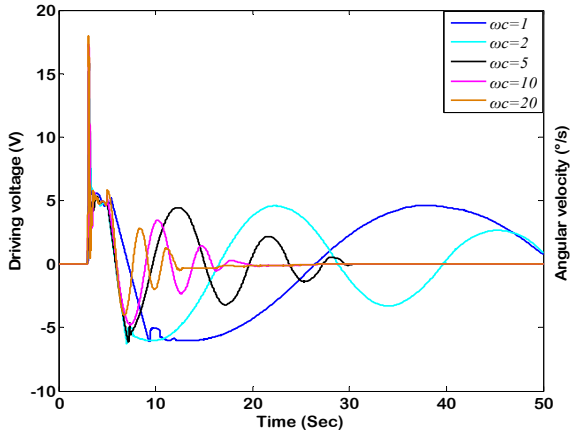

(c) Driving voltage.

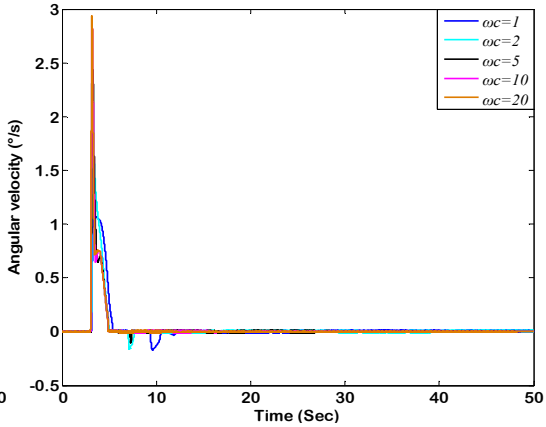

(d) Angular velocity.

Fig. 5. The system responses of theodolite angular position tracking with different ω_c.

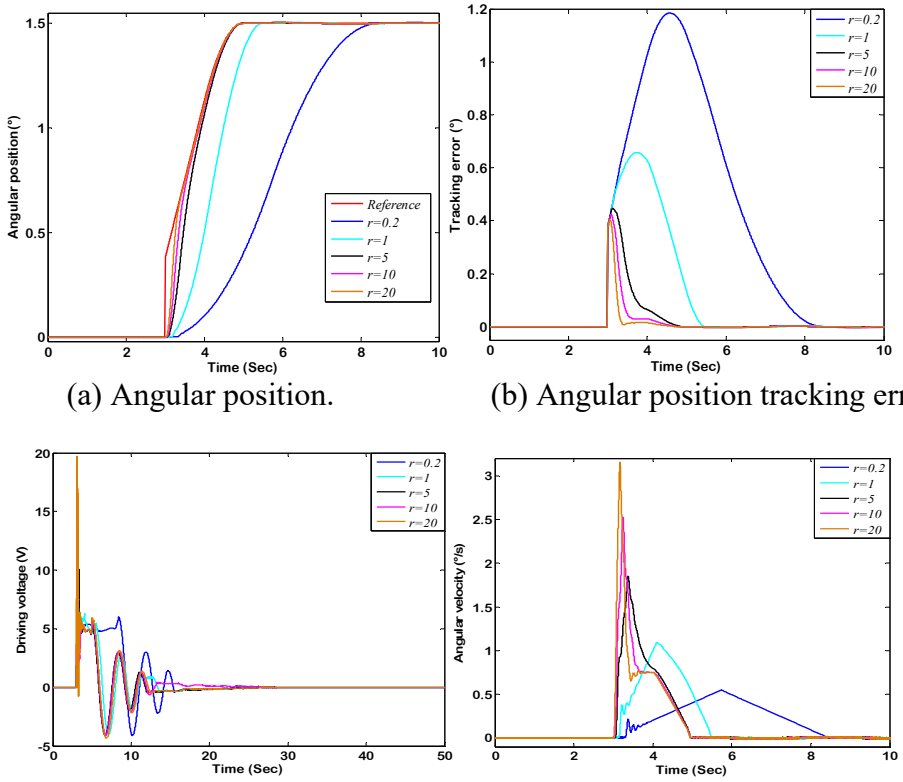

(a) Angular position. (b) Angular position tracking error.

(c) Driving voltage. (d) Angular velocity.

Fig. 6. The system responses of theodolite angular position tracking with different *r*.

4.1 ADRC Parameters Tuning

ADRC parameters are closely related to the control performance of the whole system. The main ADRC parameters to be tuned are as follows,

1) ESO: β_1, β_2, β_3; 2) NLSEF: k_p, k_d ;3) TD: r

$L=[\beta_1, \beta_2, \beta_3]^T$ is the observer gain vector. Using the bandwidth-parameterization method given by Ref. [22], all of the observer eigenvalues are $-\omega_0$, whose absolute value is the observer bandwidth, we obtain

$$L = [3\omega_0, 3\omega_0^2, \omega_0^3] \tag{19}$$

A properly tuned ω_0 must be larger than the state frequency to estimate effectively the state and disturbance. By adopting a designed ESO, outputs y and $\dot{y}$ and disturbance f can be estimated precisely. Parameters r, k_p, and k_d are fixed for 16, 25, 10 and ω_0 is set as 5, 10 and 20. The system responses of theodolite angular position tracking with different ω_0 are shown in Fig. 4. In this part, being different from the rigid step input signal, motion trajectory planning with maximum speed of 0.3°/s is used to obtain a smooth climbing curve of angular position to improve tracking performance under ADRC law.

From the Fig. 4, we can know that the bigger ω_0 improves the system tracking speed. When ω_0 is 20, the time of system convergence is about 28s, but ω_0 for 5 or 10 cannot realize it. Meanwhile, we can find the big ω_0 amplifies the noise to make driving voltage chattering. So the parameter ω_0 is chosen through considering both the system convergence time and the controller chattering.

As proportional and differential coefficients of NLSEF, k_p and k_d are selected as $k_p=2\omega_c$ and $k_d=\omega_c^2$ based on the bandwidth-parameterization method, where ω_c is the controller bandwidth. While r and ω_0 are fixed for 16 and 15, ω_c is set as 1,2,5,10, and 20, respectively. The system responses of the theodolite angular position tracking with different ω_c are shown in Fig. 5.

From Fig. 5, a large ω_c has a good position tracking performance. The better response speed can be gotten with a larger ω_c. For instance, the convergence time is about 12.5s, when ω_c is for 20. Comparatively, the convergence time for the others is increased greatly. Besides, a large ω_c can decrease the system overshoot and angular velocity undulation. When ω_c is 1, the system overshoot

as maximum value can reach 33%. Angular velocity undulation is also important character for theodolite rotating servo system. However, a large ω_c can breach the stability of the control signal. When ω_c is 20, the maximum value of driving voltage is about 18.2V, which is difficult to bear for the rated motor voltage 9V. According to the experience, the observer bandwidth ω_0 should be larger than the controller bandwidth ω_c so that the observer can follow the controller rationally considering different impacts: system response speed, position tracking overshoot, angular velocity undulation, and control voltage.

r is the parameter of TD, which influences the convergence speed of system response directly. To explain the impact principle of r, contrast experiments are carried out. While ω_c and ω_0 are fixed for 20 and 15, r is set as 0.2,1,5,10 and 20, respectively. The system responses of theodolite angular position tracking with different r are shown in Fig. 6.

Some main performance parameters comparison of different r experimental results is listed in the Tab.2. Thought reading it, we can know the performance change with different r clearly.

Tab. 2 The main performance parameters comparison of different r

r	Max. velocity (°/s)	Convergence time (s)	Max. position tracking error (°)	Max. control value (V)
0.2	0.548	16.5	1.18	7.37
1	1.091	14	0.66	8.85
5	1.802	5	0.446	12.16
10	2.342	5	0.423	15.32
20	3.133	5	0.405	19.705

Generally speaking, parameters tuning of ADRC is very important to obtain a good control performance of system, and it is also a litter difficult. In the process of experimental simulation, we can find some rules to choose the parameters of ADRC. Parameters tuning procedure of ADRC can be given in the Fig. 7.

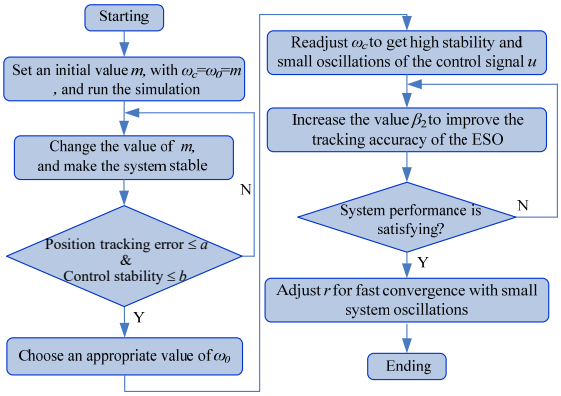

Fig. 7. The parameters tuning procedure of ADRC.

To be brief, ω_c, ω_0, and r are choosen respectively. Then, fine adjustment for some parameters to improve the whole control performance of the system.

5. Design of NTSM-ADRC based on PSO

In order to improve the control performances of the rotating servo system furthermore, NLSEF of ADRC adopts NTSM control method to enhance the system robustness and to shorten the convergence time of the system states. For system (7), the conventional NTSM is described by the following terminal sliding mode surface function, [23]

$$s = x_1 + \frac{1}{\beta} x_2^{p/q} \tag{20}$$

where β >0, and p and q are the positive odd integers satisfying $q< p< 2q$.

Based on the sliding mode surface function (20), an improved NTSM controller based the reaching law is designed as follows, [24]

$$u_0 = -b^{-1}[f(x) + \beta \frac{q}{p} x_2^{2-p/q} + ks + (l_g + \eta)\mathrm{sgn}(s)] \tag{21}$$

where η >0, is a constant. $d(x,t)$ is the uncertainty and disturbance satisfying $|d(x,t)|< l_g$, and l_g>0.

The controller can ensure the NTSM occurs. Analyzing the NTSM surface function (20), we can know that both the system states x_1 and x_2 converge to the target signals in the finite time.

Here, we choose the integral time absolute error (ITAE) performance index as the minimal target function of parameters optimization. The particle position, the particle velocity and the target function can be expressed as follows,

$$v_{t+1} = \omega v_t + c_1 r_1 (P_t - l_t) + c_2 r_2 (G_t - l_t) \tag{22}$$

$$l_{t+1} = l_t + v_{t+1} \tag{23}$$

$$W = k\int_0^\infty t|e(t)|tdt \tag{24}$$

where l and v represent the particle position and the particle velocity; ω is the inertia factor; c_1 and c_2 are the acceleration constants; r_1 and r_2 are the random numbers from [0,1]; P_t is the optimization position of the single particle before now; G_t is the optimization position of the whole particle swarm before now; W is the fitness value, that is ITAE value; is the gain coefficient; $e(t)$ is the system error.

The optimization process of NTSM-ADRC method by PSO can be seen in Fig. 8.

To explain the superiority of NTSM-ADRC with PSO, we carry out the system tracking experiment comparing with the convention ADRC method. The tracking target is set for y_r=0.4°. The same parameters of TD and ESO are the same as those of the above rigid step input signal: T=0.001, r=16, h_0=0.001, δ=0.2, α_1=0.75 and α_2=1.25; The ESO parameters of the convention ADRC method are given as follows: β_1=40, β_2=1000, β_3=8000; The NELSF parameters of the convention ADRC method are set as follows: k_p=25, k_d=10, b_0=1.7. The NTSM parameters of the proposed ADRC method are set as follows: β=5, p=5, q=3, k=10, l_g=0.78 and η =0.2; The parameters of PSO are given as follows: iteration number G=250, swarm size m=30, dimension number D=3, inertia factor ω=0.6 and acceleration constants c_1=c_2=1.5. After 250 steps iteration, the curves of the fitness W can be displayed in Fig. 9; The angular tracking performance comparisons under proposed ADRC method and convention ADRC method are shown in Fig. 10a.

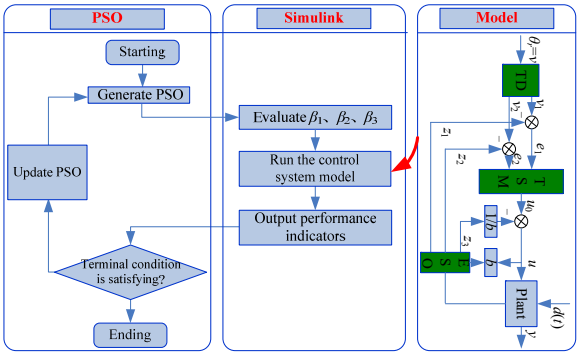

Fig. 8. The optimization process sketch map of NTSM-ADRC method by PSO.

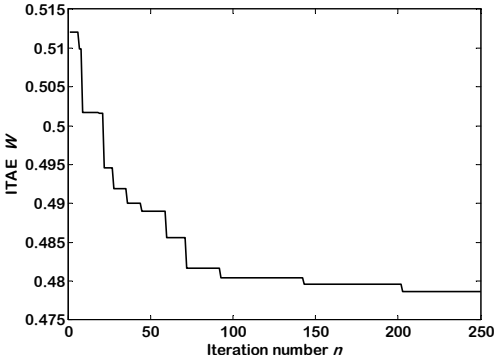

Fig. 9. The varying curves of W with PSO.

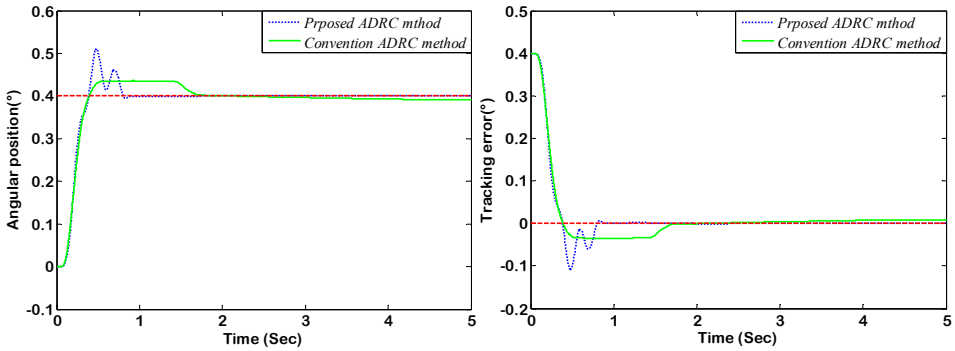

(a) Angular position tracking performance (b) Angular position tracking error

Fig. 10. The performance comparisons under proposed ADRC and convention ADRC method.

From Fig. 9, the performance index ITAE reduces unceasingly in the process of the controller optimization to find the better parameters. The parameters after tuning based on PSO are gotten as follows: β_1=31.2358, β_2=141.5187, β_3=6579.2368.

As shown by Fig.10b, the proposed NTSM-ADRC obtains satisfying dynamic and static performance in the presence of both load variation and strongly nonlinear friction torque. In the beginning stage of the state tracking, the response curves are similar. Although the overshoot value using the proposed method is larger than that using the convention ADRC, it reduces rapidly to achieve the system states convergence about 0.5s. The total convergence time is about 0.92s, which is much less than the convergence time of the convention ADRC. Enlarging the simulation time for 50s of the convention ADRC method, the overshoot time is about 1.72s and the states convergence time is about 26s. From simulation results, we can also know that the steady error with the designed control method is reduced to 1.2×10^{-4} from 5.7×10^{-3} with the convention ADRC method due to NTSM and PSO.

6. Conclusions and Further Remarks

This paper has presented a practical application of ADRC for precision rotating servo system of electronic theodolite with the internal nonlinear dynamics and external disturbance. To account for system dynamics variations, the ADRC is thus employed to estimate and compensate for them. Considering the different reference input signals and the different perturbation conditions of the system parameters, the tracking performance of the system is analyzed. PSO and NTSM control are introduced into ADRC to optimize the controller parameters and to improve the performances of the theodolite rotating system. Simulation results have demonstrated the effectiveness of ADRC.

References

[1]. Yang L B, Yan-Hong L I, Wang J, et al. Application of multi-lens image stitching to opto-electronic theodolites[J]. Optics & Precision Engineering, 18(5):1048-1053, (2010).

[2]. Sprogis K R, Raudino H C, Hocking D, et al. Complex prey handling of octopus by bottlenose dolphins (Tursiops aduncus) [J]. Marine Mammal Science, 33(3) 2017.

[3]. Xie M, Ma C, Liu K, et al. The application of active polarization imaging technology of the vehicle theodolite[J]. Optics Communications, 433:74-80, (2019).

[4]. Denos B R, Sommer D E, Favaloro A J, et al. Fiber Orientation Measurement from Mesoscale CT Scans of Prepreg Platelet Molded Composites[J]. Composites Part A: Applied Science and Manufacturing, (2018).

[5]. J. A. Ratches, “Review of current aided/automatic target acquisition technology for military target acquisition tasks,” Opt. Eng. 50(7), 072001 (2011).

[6]. Unruh S, Schneider P, Sluse D. Ambiguities in gravitational lens models: the density field from the source position transformation[J]. Astronomy & Astrophysics, 601. (2016).

[7]. K. M. Wang, X. S. Guo, Z. F. Zhou, and P. C. Pu, "Research of accurate theodolite rotating technology based on PIDNN," Comput. Meas. & Contr. 20(11), 3042-3047 (2012).

[8]. Z. Gao, and R. R. Rhinehart, "Theory vs. practice forum," in Proceedings of American Control Conference, Boston, MA, pp. 1341-1349 (2004).

[9]. H. Feng, and S. Li, "The stability for a one-dimensional wave equation with nonlinear uncertainty on the boundary," Nonlinear Anal. 89, 202-207 (2013).

[10]. H. Ran M, Wang Q, Dong C. Stabilization of a class of nonlinear systems with actuator saturation via active disturbance rejection control[J]. Automatica,, 63:302-310,(2016).

[11]. Liu F, Li Y, Cao Y, et al. A Two-Layer Active Disturbance Rejection Controller Design for Load Frequency Control of Interconnected Power System[J]. IEEE Transactions on Power Systems, 31(4):1-2(2015).

[12]. Yuefei Z, Xiaoyong Z, Li Q, et al. Active Disturbance Rejection Controller for Speed Control of Electrical Drives Using Phase-locking Loop Observer[J]. IEEE Transactions on Industrial Electronics:1-1(2018).

[13]. Chen Q, Ren X, Na J, et al. Adaptive robust finite-time neural control of uncertain PMSM servo system with nonlinear dead zone[J]. Neural Computing and Applications, (2016).

[14]. Liu J, Hong-Wen L I, Deng Y T. PMSM sliding-mode control based on novel reaching law and disturbance observer[J]. Chinese Journal of Engineering, (2017).

[15]. Hosseini-Pishrobat M, Keighobadi J. Robust output regulation of a triaxial MEMS gyroscope via nonlinear active disturbance rejection[J]. International Journal of Robust & Nonlinear Control, 28(5) (2018).

[16]. H. L. Xing, J. H. Jeon, K. C. Park, et al. "Active disturbance rejection control for precise position tracking of ionic polymer–metal composite actuators," IEEE/ASME Trans. Mech. 18(1): 86-95 (2013).

[17]. Li H, Chen G, Huang T, et al. High-Performance Consensus Control in Networked Systems with Limited Bandwidth Communication and Time-Varying Directed Topologies[J]. IEEE Transactions on Neural Networks and Learning Systems, 28(5):1-12. (2016).

[18]. J. Han, "From PID to active disturbance rejection control," IEEE Trans. Indu. Elec. 56(3), 1-7 (2009).

[19]. Van M, Mavrovouniotis M, Ge S S. An Adaptive Backstepping Nonsingular Fast Terminal Sliding Mode Control for Robust Fault Tolerant Control of Robot Manipulators[J]. IEEE Transactions on Systems Man & Cybernetics Systems, PP (99):1-11(2017).

[20]. Xie Y, Yungang L I, She L, et al. A Discrete Second-Order Nonlinear Tracking-Differentiator Based on Boundary Characteristic Curves[J]. Information & Control, (2014).

[21]. Lei W, Astolfi D, Marconi L, et al. High-gain observers with limited gain power for systems with observability canonical form[J]. Automatica, 2017, 75(C):16-23.

[22]. Z. Gao, "Scaling and bandwidth-parameterization based controller tuning," in Proc. 2003 American Control Conf., 6, 4989-4996 (2003).

[23]. Y. Feng, S. Bao, and X. H. Yu, "Design method of non-singular terminal sliding mode control systems," Control and Decision, 17(2), 194-198 (2002).

[24]. W. W. Zhang and J. Wang, “Nonsingular Terminal sliding model control based on exponential reaching law,” Control and Decision, 27(6), 909-913 (2012).

[25]. Y Bista S R, Giordano P R, Chaumette F. Combining line segments and points for appearance-based indoor navigation by image based visual servoing[C]// IEEE/RSJ International Conference on Intelligent Robots & Systems. (2017).